RESEARCH ARTICLE

FASEB BioAdvances WILEY

Upregulated expression of a subset of genes in *APP*;*ob/ob* mice: Evidence of an interaction between diabetes-linked obesity and Alzheimer's disease

Mitsuru Shinohara[1,2] | **Masataka Kikuchi**[3] | **Miyuki Onishi-Takeya**[4] | **Yoshitaka Tashiro**[1] | **Kaoru Suzuki**[1] | **Yasuhiro Noda**[1] | **Shuko Takeda**[5] | **Masahiro Mukouzono**[5] | **Seiichi Nagano**[6] | **Akio Fukumori**[1,2] | **Ryuichi Morishita**[5] | **Akihiro Nakaya**[3] | **Naoyuki Sato**[1,2]

[1]Department of Aging Neurobiology, Center for Development of Advanced Medicine for Dementia, National Center for Geriatrics and Gerontology, Obu, Aichi, Japan

[2]Department of Aging Neurobiology, Graduate School of Medicine, Osaka University, Osaka, Japan

[3]Department of Genome Informatics, Graduate School of Medicine, Osaka University, Osaka, Japan

[4]Department of Geriatric Medicine, Graduate School of Medicine, Osaka University, Osaka, Japan

[5]Department of Clinical Gene Therapy, Graduate School of Medicine, Osaka University, Osaka, Japan

[6]Department of Neurology, Graduate School of Medicine, Osaka University, Osaka, Japan

Correspondence
Naoyuki Sato, Head of the Department of Aging Neurobiology, Center for Development of Advanced Medicine for Dementia, National Center for Geriatrics and Gerontology, 7-430, Morioka, Obu, Aichi 474-8511, Japan.
Email: nsato@ncgg.go.jp

Abstract

Clinical studies have indicated that obesity and diabetes are associated with Alzheimer's disease (AD) and neurodegeneration. However, the mechanism by which obesity/diabetes and AD interact with each other and contribute to dementia remains elusive. To obtain insights into their interaction at molecular levels, we performed gene expression analysis of *APP*;*ob/ob* mice, which were generated by crossing transgenic AD model mice (APP23 mice) with *ob/ob* mice, which are obese and mildly diabetic. The Aβ level in these mice was reduced compared with that in pure *APP* mice. However, we identified a cluster of genes (cluster 10) upregulated in *APP*;*ob/ob* mice but not in either *APP* or *ob/ob* mice. Interestingly, genes upregulated in the human AD brain were enriched in cluster 10. Moreover, genes in cluster 10 formed a network and shared upregulated genes with a cell model of neurodegeneration and other models of neurological disorders such as ischemia and epilepsy. In silico analyses showed that serum response factor (SRF), recently identified in a single-cell analysis

of human brains as a transcription factor that can control the conversion from healthy cells to AD cells, might be a common transcriptional regulator for a subset of cluster 10 genes. These data suggest that upregulation of genes uniquely associated with *APP*;*ob/ob* mice is an evidence of the interaction between obesity/diabetes and AD.

KEYWORDS

Alzheimer's disease, animal models, diabetes, interaction, obesity

1 | INTRODUCTION

Emerging evidence suggests that diabetes is associated with Alzheimer's disease (AD) and neurodegeneration,[1–7] although the mechanisms underlying this association remain elusive.[8,9] Several neuropathological studies have reported that diabetes is not associated with amyloid accumulation or neurofibrillary tangles (NFT) formation,[10–13] while some studies have indicated that amyloid accumulation is lower in AD patients with diabetes than in those without diabetes.[14–17] Diabetes exacerbates frontal and temporal lobe atrophy, and patients with diabetes present clinically with decreased executive function and processing speed.[18] Obesity, which is closely linked to diabetes, also increases the risk of dementia.[19] The FINGER study showed that multidomain interventions, such as exercise, diet, cardiovascular control, and cognitive training, ameliorate cognitive functions such as executive function and processing speed in subjects with obesity and other risk factors for dementia.[20] Therefore, cognitive function exacerbated by obesity/diabetes might be preserved by exercise, diet, and cardiovascular control, although the effect of cognitive training in the FINGER study cannot be excluded. Therefore, determining the mechanisms by which obesity/diabetes increase the risk of dementia would provide insight into the development of novel therapeutics for dementia.

To clarify the molecular mechanisms by which obesity/diabetes modify cognitive function, we performed gene expression analysis of amyloid precursor protein (*APP*);*ob/ob* mice, which are AD model mice with diabetes-linked obesity.[21,22] We generated *APP*;*ob/ob* mice by crossing transgenic AD model mice (APP23 mice) with *ob/ob* mice. APP23 mice overexpress *APP* with Swedish familial AD mutations and exhibit amyloid deposition.[23] *Ob/ob* mice are leptin-deficient and become obese and diabetic.[24–26] We previously observed that *APP*;*ob/ob* mice exhibit cognitive dysfunction at a young age and neurodegeneration in later life.[21,27] Here, we identified a unique set of genes that are upregulated in the mouse brain only when obesity and ectopic *APP* expression are combined. Indeed, these genes exhibit substantial overlap with genes upregulated in the hippocampus of humans with AD. Moreover, these genes are upregulated in a cell model of neurodegeneration[28] and in animal models of

neurological disorders, such as ischemia models[29] and an epilepsy model,[30] indicating the common roles of these genes in neurodegeneration. These data suggest that upregulation of a subset of genes in *APP*;*ob/ob* mice is the evidence of the interaction between obesity/diabetes and AD.

2 | MATERIALS AND METHODS

2.1 | Animals

All animal experiments were performed in compliance with the Guidelines for the Care and Use of Laboratory Animals of Osaka University School of Medicine. Animals were maintained at room temperature ($25 \pm 2°C$) under a standard 12/12-h light–dark cycle, with free access to water and standard chow. All mice were on the same genetic background (C57BL/6 J) and were housed without enrichment structures in a specific pathogen-free environment. *APP*;*ob/ob* mice were generated by crossbreeding APP23 mice with *ob/ob* mice (Charles River Japan Inc., Japan) as we previously described.[21] Male heterozygous APP23 (*APP*) mice were crossbred with female heterozygous *ob/+* mice to generate *APP*;*ob/+* and *ob/+* founder mice. We then intercrossed these mice to obtain *APP*;*ob/ob*, *APP*, *ob/ob*, and wild-type littermate mice. We used real-time PCR to assess *APP* expression in the brains of these mice. Male 16-month-old mice were used for analysis.

2.2 | Tissue collection and sample preparation

Mice were anesthetized with xylazine and ketamine (20 and 100 mg/kg, respectively). After transcardial perfusion with PBS supplemented with complete protease inhibitor cocktail (Nacalai Tesque), the brain was removed and divided along the sagittal plane; then, the right hemisphere (cortical and hippocampal areas) was snap frozen in liquid nitrogen and stored at −80°C until biochemical analysis. The left hemisphere was fixed with 4% paraformaldehyde overnight and was then embedded in paraffin for histological

analysis. For biochemical analysis, tissues were pulverized in a prechilled (on dry ice) BioPulverizer (BioSpec) and homogenized with a polytron homogenizer (Kinematica) at a ratio of 20 mL/g wet weight brain tissue in ice-cold RIPA lysis buffer (Millipore) containing 0.1% SDS and complete protease inhibitor cocktail (Roche) on ice. After centrifugation at $100,000 \times g$ for 1 h at 4°C, the supernatant was collected and used for biochemical analysis. The order of sample preparation and subsequent analyses was randomly assigned independent of genotype.

2.3 | RNA-seq

Total RNA was extracted using an RNeasy Lipid Tissue Mini Kit (Qiagen). mRNA was isolated from purified total RNA using a Micropoly(A)Purist[TM] mRNA Purification Kit (Thermo Fisher Scientific). cDNA was reverse transcribed from mRNA after fragmentation using a SOLID[TM] Total RNA-Seq Kit (Thermo Fisher Scientific). The quality of RNA and cDNA was assessed with a bioanalyzer (Agilent). Sequencing was performed using a next-generation sequencing system (5500xl SOLiD System, Thermo Fisher Scientific).

2.4 | Classification of differentially expressed genes (DEGs)

We selected 2543 DEGs with a $q < 0.05$ in a comparison between any two groups. Next, we used agglomerative hierarchical clustering based on Ward's method and the Euclidean distance to separate the DEGs into 10 clusters. The number of clusters was set to 10 based on the gap statistic (Figure S1).[31] All analyses were performed in R.[32]

2.5 | Enrichment analysis of cell-specific genes

To analyze the enrichment of cell-specific genes in each cluster, we used publicly available RNA-seq datasets of neurons, astrocytes, oligodendrocyte precursor cells (OPCs), newly formed oligodendrocytes (NFOs), myelinating oligodendrocytes (MOs), microglia, endothelial cells, and pericytes from the mouse cerebral cortex.[33] We used seven of these eight cell types (all except pericytes). Among 22,458 genes, we selected 10,952 genes with gene expression fold changes of >5 when mean values were compared between any two cell types. Next, we used agglomerative hierarchical clustering based on Ward's method and the Euclidean distance to separate these 10,952 genes into 20 clusters. Among the 20 clusters, we manually curated 7 that generally showed a

prominent peak in a specific cell type (Figure S2A). NFOs and MOs were integrated into one cluster. We finally defined the genes in each cluster as cell-specific genes (Figure S2B). To examine the extent of overlap between the cell-specific genes and the genes in a cluster, we calculated the p-value using a hypergeometric distribution test and the fold enrichment ratio (FER), as follows:

$$P(X = x) = \frac{\binom{m}{x}\binom{N-m}{n-x}}{\binom{N}{n}},$$

$$FER = \frac{x}{E},$$

$$E = \frac{mn}{N},$$

where x is the number of genes overlapping between the set of cell-specific genes and the set of genes in a cluster, m is the number of cell-specific genes, n is the number of genes in a cluster, N is the total number of genes, and E is the expected value. An FER of greater than 1 indicates that the overlap between the cell-specific genes and the genes in a cluster is higher than expected.

2.6 | Enrichment analysis of DEGs in the human AD brain

We used AlzData to identify the genes up- or downregulated in the human AD brain.[27] AlzData is a database that stores statistical meta-analysis results analyzed in the entorhinal cortex (EC), frontal cortex (FC), hippocampus (HIP), and temporal cortex (TC). Gene expression levels were analyzed with a linear regression model including age and sex as covariates. We downloaded processed data from AlzData and used the log2-fold change (log2FC) values and FDR-adjusted p-values in the processed data. To examine the extent of overlap between the DEGs (adjusted $p < 0.05$) in the human AD brain and the genes in a cluster, we calculated the p-values with a hypergeometric distribution test and determined the FER.

2.7 | Prediction of potential regulators

To predict transcription factors (TFs) that may regulate the expression levels of the genes in cluster 10, we used oPOS-SUM (version 3.0) to search for conserved TF-binding sites

in regions ±5 kb from the transcription start sites of the genes.[34] The TFs exhibited a z-score of ≥10 and a Fisher score of ≥7 (default values) in "Mouse Single Site Analysis" in oPOSSUM.

2.8 | Quantitative real-time PCR

Total RNA was purified from brain tissues using an RNeasy Lipid Tissue Mini kit (QIAGEN) and was then eluted in nuclease-free water and stored at −80°C. Reverse transcription was performed using ReverTra Ace® qPCR RT Master Mix (TOYOBO). Real-time PCR was conducted with Luna Universal qPCR Master Mix (New England Biolabs) in an i1000 thermal cycler (Bio-Rad) to detect the mRNA levels of glial fibrillary acidic protein (*Gfap*), myelin-associated glycoprotein (*Mag*), proteolipid protein 1 (*Plp1*), DNAX-activation protein 12 (*Dap12*), triggering receptor expressed on myeloid cells 2 (*Trem2*), C-C motif chemokine ligand 3 (*Ccl3*), C-C motif chemokine ligand 4 (*Ccl4*), BTG anti-proliferation factor 2 (*Btg2*), cysteine-rich angiogenic inducer 61 (*Cyr61*), an AP-1 transcription factor subunit (*JunB*), lanosterol synthase (*Lss*), dual specificity phosphatase 1 (*Dusp1*), *Fos* (an AP-1 transcription factor subunit), neuronal PAS domain protein 4 (*Npas4*), β-tubulin (*Tubb4a*), and β-actin. The following primers were used: *β-actin* forward primer: AGTGTGACGTTGACATCCGTA and reverse primer: GCCAGAGCAGTAATCTCCTTC; *Trem2* forward primer: TGCTGGCAAAGGAAAGGT and reverse primer: GTTGAGGGCTTGGGACAGG; *Dap12* forward primer: GTTGACTCTGCTGATTGCCCT and reverse primer: CCCTTCCGCTGTCCCTTGA (all obtained from Integrated DNA Technologies); *Btg2* forward primer: ATGAGCCACGGGAAGAGAAC and reverse primer: GCCCTACTGAAAACCTTGAGTC; *Cyr61* forward primer: CTGCGCTAAACAACTCAACGA and reverse primer: GCAGATCCCTTTCAGAGCGG; *JunB* forward primer: TCACGACGACTCTTACGCAG and reverse primer: CCTTGAGACCCCGATAGGGA; *Lss* forward primer: TCGTGGGGGACCCTATAAAC and reverse primer: CGTCCTCCGCTTGATAATAAGTC; *Dusp1* forward primer, GTTGTTGGATTGTCGCTCCTT and reverse primer: TTGGGCACGATATGCTCCAA; *Fos* forward primer: CGGGTTTCAACGCCGACTA and reverse primer: TTGGCACTAGAGACGGACAGA; *Npas4* forward primer: AGCATTCCAGGCTCATCTGAA and reverse primer, GGCGAAGTAAGTCTTGGTAGGATT; *β-tubulin* forward primer: CACCTGCAAGCCGGTCAAT and reverse primer: TCCCCATGATAGGTCCCAGTG; *Gfap* forward primer: CGGAGACGCATCACCTCTG and reverse primer: AGGGAGTGGAGGAGTCATTCG; *Ccl3* forward primer: TTCTCTGTACCATGCACTCTGC and reverse primer: CGTGGAATCTTCCGGCTGTAG; *Ccl4* forward primer:

TTCCTGCTGTTTCTCTTACACCT and reverse primer: CTGTCTGCCTCTTTTGGTCAG; *Mag* forward primer: CTGCCGCTGTTTTGGATAATGA and reverse primer: CATCGGGGAAGTCGAAACGG; and *Plp1* forward primer: CCAGAATGTATGGTGTTCTCCC and reverse primer: GGCCCATGAGTTTAAGGACG. The relative expression levels were quantified and analyzed using Bio-Rad iCycler iQ software (Bio-Rad). Relative mRNA levels were calculated using the ΔΔCt method with *β-actin* or *β-tubulin*, as appropriate, as the internal control for each specific gene amplification reaction.

## 2.9 | ELISA and other biochemical assays

The levels of GFAP and CD11b were measured using ELISA as previously described.[35] Colorimetric quantification was performed with an iMark plate reader (Bio-Rad) after incubation with horseradish peroxidase (HRP)-conjugated Avidin-D (Vector) or anti-rabbit IgG (H + L), HRP conjugate (Promega), and the 3,3′,5,5′-tetramethylbenzidine substrate (Sigma-Aldrich). For measurement of Aβ, brain samples were homogenized in 5 volumes (w/v) of 1% Triton X-100 in 25 mM Tris-buffered saline (TBS) (pH 7.9) containing complete protease inhibitor (Roche) using a Teflon-glass homogenizer. After incubation on ice for 3 h, the homogenate was centrifuged at $100,000 \times g$ for 20 min at 4°C. The supernatant was saved as the Triton X-100 soluble fraction. The resulting pellet was mixed with 5 volumes (w/v) of 5 M guanidine HCl, sonicated, and incubated for 2 h at room temperature. The mixtures were diluted with TBS and centrifuged at $4000 \times g$ for 20 min at 4°C. The supernatants were neutralized before loading onto the ELISA plates. Human/rat Aβ40 and Aβ42 levels were measured by ELISA following the manufacturer's instructions (Wako).

2.10 | Immunohistochemical staining

Mouse brains were fixed as described in the "Tissue collection and sample preparation" section. Brain samples were embedded in paraffin and sliced into 10-μm-thick sections. Brain sections were submerged in EDTA buffer (1 mM, pH 8.0) and autoclaved for antigen retrieval. The sections were immersed in 95% formic acid for Aβ staining. Endogenous peroxidase activity was quenched by incubating the sections with hydrogen peroxide. Sections were incubated with primary antibodies at 4°C overnight; we used an anti-Aβ (6E10, epitope: 3–8 aa of Aβ) antibody (Merck). Sections were then incubated with an HRP-conjugated secondary antibody and diaminobenzidine reaction mixture (Vector Laboratories). The stained sections were evaluated under a microscope (BZ-X810, Keyence).

FIGURE 1 Classification of DEGs. (A) Hierarchical clustering and heatmap of wild-type (WT), APP23 (*APP*), diabetic (*ob/ob*), and *APP*;*ob/ob* mice. The expression levels of each gene were averaged over biological replicates (*n* = 3 mice/group) and were transformed into z-scores for the four mouse genotypes. Each row and each element represent each gene and the z-score for that gene, respectively. In this analysis, 2543 genes that were significantly differentially expressed (FDR <0.05) in at least one comparison between mouse genotypes were analyzed. The colors to the left of the heatmap indicate each cluster. (B) Detailed gene expression patterns in each cluster shown in A. The black and red polygonal lines indicate the z-scores of the genes and their averaged z-scores, respectively. Clustering was performed using Ward's method. The number of clusters was set to 10 based on the gap statistic (Figure S1)
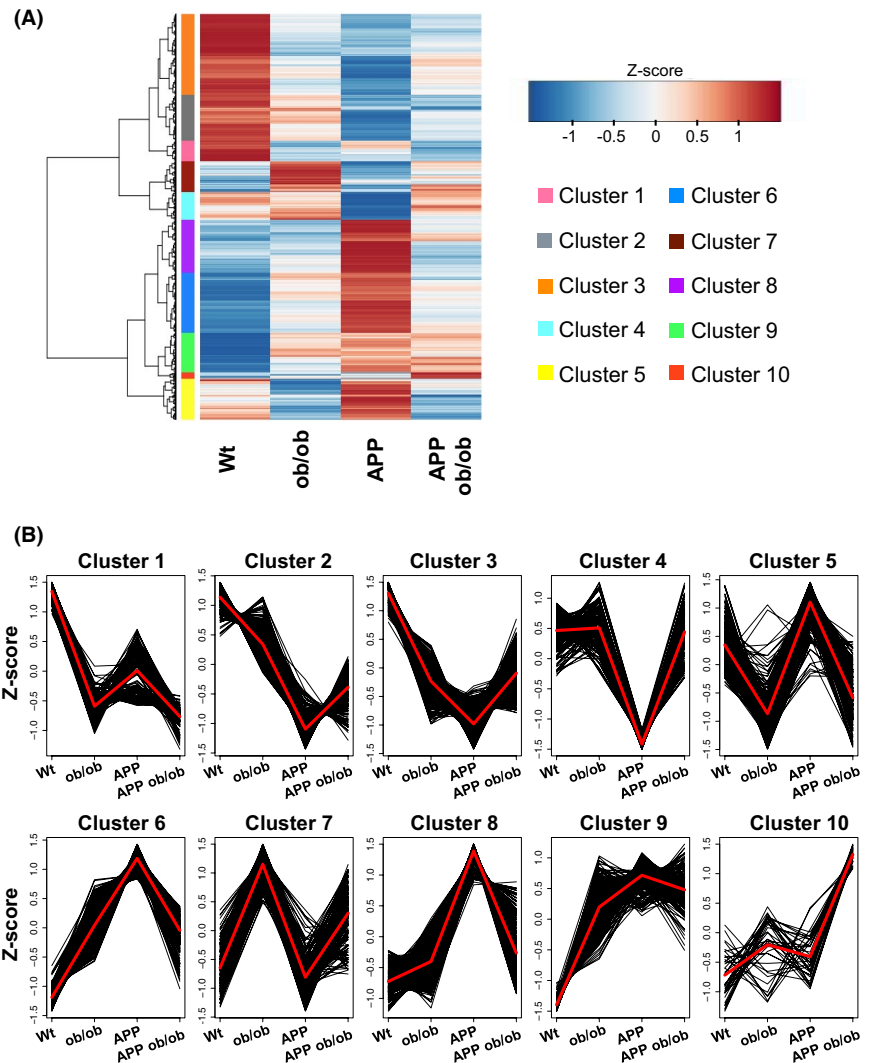
2.11 | Klüver–Barrera (KB) staining

Brain sections were treated with Luxol Fast Blue solution (Muto Pure Chemical, Japan) at 65°C overnight. The sections were chilled to room temperature, rinsed with 95% ethanol and distilled water, treated with 0.1% lithium carbonate and 70% ethanol, rinsed with distilled water and counterstained with 0.1% cresyl violet acetate solution (Muto Pure Chemicals) containing 10% acetic acid. Sections were dehydrated with 95% ethanol, cleared with xylene, and mounted with Entelan® New (Merck, USA). Histological analysis was performed using a Leica microscope (DM5000B, Leica, Wetzlar, Germany), and images of the paramedial corpus callosum in each group were acquired.

2.12 | Statistical analysis

Statistical analyses were performed using JMP Pro software (version 12, SAS Institute Inc.). All data are expressed as the means ± S.E.M. values. Two-group comparisons were performed with Student's *t*-test. Comparison of means among three or more groups was performed by analysis of variance (ANOVA) followed by the Tukey–Kramer multiple-range test. Values of *p* < 0.05 were considered to indicate significant differences.

3 | RESULTS

We previously generated an animal model reflecting the pathologic condition of both AD and diabetes-linked obesity (*APP*;*ob/ob* mice) and reported early cognitive impairment, neuroinflammation, vascular dysfunction, and insulin signalling disturbances despite a trends of reduced Aβ accumulation, especially in old age.[21] Consistent with these findings, Aβ accumulation was significantly reduced in *APP*;*ob/ob* mice compared with *APP* mice at 16 months of age, as shown by the results of both immunohistochemical staining (Figure S3A) and biochemical analyses (Figure S3B-E). This pattern might be in part due to the lower expression of *APP* in *APP*;*ob/ob* mice (Figure 3F). To characterize changes at

the molecular level in more detail, we performed RNA-seq on brain samples of these mice at this age. Gene expression analysis showed the characteristic features of each genotype. Accordingly, we classified these expression patterns into 10 clusters (Figure 1A). Clusters 1, 2, and 3 contained genes that were generally downregulated in *ob/ob*, *APP*, and *APP;ob/ob* mice compared with wild-type mice. Cluster 4 contained genes that were downregulated specifically in *APP* mice, while clusters 6 and 8 contained genes that were upregulated in *APP* mice. Notably, cluster 10 contained genes that were upregulated in *APP;ob/ob* mice but not in either *APP* or *ob/ob* mice (Figure 1B).

We next performed enrichment analysis on each gene cluster to understand the properties represented by each cluster. Enrichment analysis of gene function showed that clusters 1, 2, and 3 containing genes with reduced expression in *APP*, *ob/ob*, and *APP;ob/ob* mice were enriched with genes involved in translation and mitochondrial function (Table S1). Enrichment analysis of cell-specific genes showed that cluster 5, containing genes with downregulated expression in both *ob/ob* and *APP;ob/ob* mice (i.e., mice on the *ob/ob* background), was enriched with genes specific to oligodendrocyte and microglial cells (Figure 2). Moreover, genes specific to astrocytes and microglial cells were enriched in cluster 8, which contained genes with increased expression in *APP* mice but not in *APP;ob/ob* mice. To confirm the results of RNA-seq, we performed real-time qPCR; indeed, the levels of genes belonging to clusters 5 and 8, including the

astrocyte marker (*Gfap*), microglial-related genes (*Dap12*, *Trem2*, *Ccl3*, and *Ccl4*), and oligodendrocyte-related genes (*Mag* and *Plp1*), exhibited changes similar to those observed in the RNA-seq data (Figure 3A-G). The protein levels of an astrocyte marker (GFAP) and a microglial-related marker (CD11b) showed trends similar to those in their mRNA levels (Figure 3H and I). Notably, apparent white matter lesions were observed in *ob/ob* and *APP;ob/ob* mice, suggesting that the levels of oligodendrocyte-related genes were decreased in these mice (Figure S4).

Then, we compared our RNA-seq data with publicly available datasets of data from human AD brains and examined their overlap (Figure 4 and Table S2). Clusters 5, 6, and 8 were overrepresented with genes with upregulated expression in brains from patients with AD. On the other hand, clusters 2, 3, and 4 were enriched with genes with downregulated expression in brains from patients with AD. Interestingly, similar to clusters 5, 6, and 8, cluster 10 was enriched with genes with upregulated expression in brains from patients with AD, especially in the hippocampal area that is most vulnerable in AD patients, suggesting their critical roles in AD pathogenesis.

As the expression pattern of cluster 10 suggests an interaction between obesity/diabetes and AD, we further characterized this cluster. Cluster 10 included *Btg2*, *Cyr61*, *JunB*, *Lss*, *Dusp1*, *Fos*, and *Npas4*, which were also confirmed by real-time PCR (Figure 5A and Table S3). These genes in cluster 10 were also upregulated in a cell model
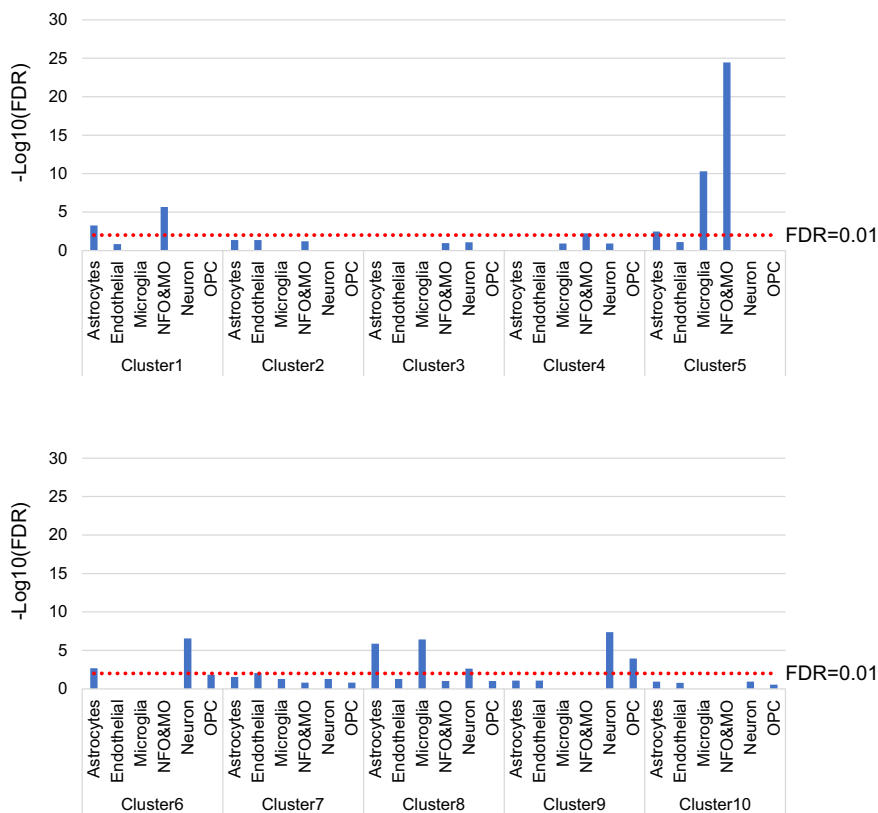

FIGURE 2 Enrichment analysis of cell-specific genes. The y-axis shows the –log10 FDR-adjusted *p*-values calculated by the hypergeometric test. Each bar shows only the –log10(FDR) with FER >1. An FER of greater than one means that the proportion of cell-specific genes is higher than the expected proportion. The red line indicates an FDR-adjusted *p*-value of 0.01. NFO: newly formed oligodendrocytes, MO: myelinating oligodendrocytes, and OPC: oligodendrocyte precursor cells

FIGURE 3 Validation of gene expression patterns for clusters 5 and 8 by real-time PCR or ELISA. The mRNA levels of *Gfap* (A), *Dap12* (B), *Trem2* (C), *Ccl3* (D), *Ccl4* (E), *Mag* (F), and *Plp1* (G) were measured using real-time PCR and were compared among the genotypes (*n* = 4–6 mice/group). The protein levels of GFAP (H) and CD11b (I) were measured using ELISA and compared among the genotypes (*n* = 4–6 mice/group). The data are presented as the adjusted means ± standard errors of the mean. **p < 0.05, **p < 0.01, and ***p < 0.001 by the Tukey–Kramer test. Wt = wild-type
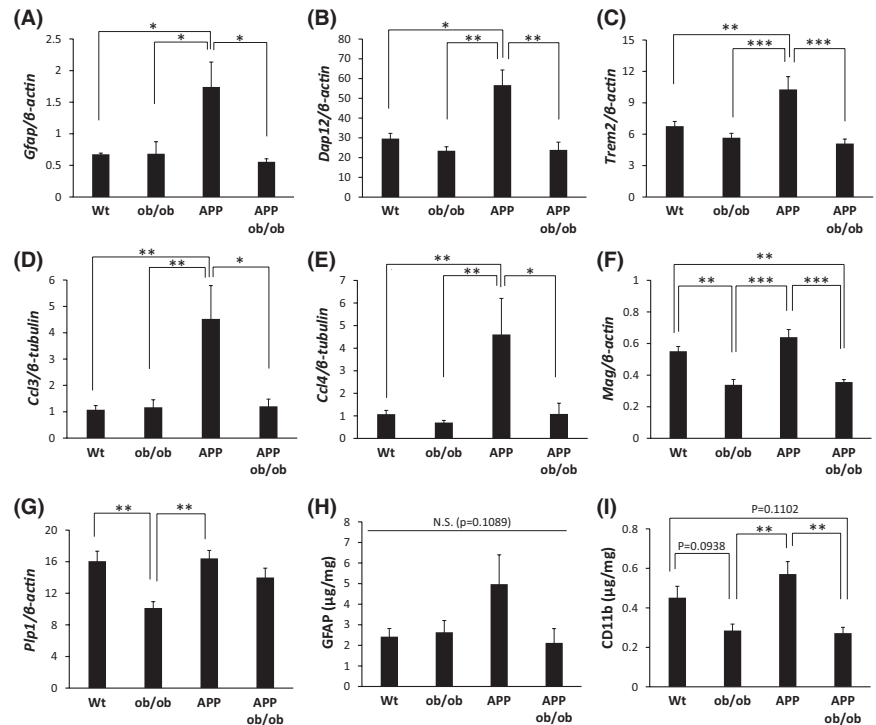
of neurodegeneration (i.e., *Btg2*, *Cyr61*, *Dusp1*, *JunB*, and *Npas4*[28]) and animal models of neurological disorders, such as ischemia models (i.e., *Btg2*, *Cyr61*, *Dusp1*, *Fos*, *JunB*, and *Npas4*[29]), and an epilepsy model (i.e., *Btg2*, *Cyr61*, *Dusp1*, *Fos*, *JunB*, and *Npas4*[30]), suggesting their important roles in general neurodegenerative diseases. Finally, we used bioinformatics approaches to determine whether cluster 10 genes had a common transcriptional regulator. Via oPOSSUM software,[34] we found that four TFs—serum response factor (SRF), specificity protein 1 (SP1), insulinoma-associated protein 1 (INSM1), and myeloid zinc finger 1 (MZF1)—can regulate the expression of genes in cluster 10. In particular, genes targeted by SRF were the most abundant (Figure 5B and Table S4), and the significant enrichment of SRF binding in the upstream region of cluster 10 genes was confirmed in the ChIP-Atlas database (Table S5).

4 | DISCUSSION

While clinical studies have indicated associations between obesity/diabetes and dementia, the mechanisms by which obesity/diabetes increase the risk of dementia are incompletely understood. Previously, we showed that *APP*;*ob/ob* mice, AD model mice with diabetes-linked obesity, exhibit cognitive dysfunction at a young age and inflammatory and vascular changes at 12 months of age.[21] In this study, we sought to investigate the precise mechanisms involved in these changes by quantifying gene expression in the brains of *APP*;*ob/ob* mice at 16 months of age. Notably, the Aβ level was reduced in *APP*;*ob/ob* mice compared with *APP* mice,

likely to be partially due to the lower expression of *APP* at this age (Figure S3). However, we observed upregulated expression of a subset of genes in *APP*;*ob/ob* mice, which might illuminate the molecular mechanism underlying the interaction between obesity/diabetes and AD.

Genes specific to oligodendrocytes and microglial cells were downregulated in both *ob/ob* and *APP*;*ob/ob* mice (i.e., mice on the *ob/ob* background). These results are consistent with clinical evidence indicating that diabetes is associated with reduced white matter volume[36] as well as with reductions in hippocampal volume[1,36] and gray matter volume.[37] In addition, diabetes is associated with aberrant functional connectivity of the posterior cingulate cortex with the temporal gyrus[38] and frontal gyrus,[39] suggesting white matter abnormalities occur in diabetes. In this study, we found that the expression of Mag, a myelin-associated glycoprotein, was reduced in both *ob/ob* and *APP*;*ob/ob* mice (Figure 3). Mag is thought to be involved in myelination, and deficiency of this protein results in demyelinating leukodystrophy in humans.[40] Diabetes is associated with dysregulation of macrophages in the peripheral system in humans[41] and animal models.[42] Indeed, diabetes increases susceptibility to infection[43] and impairs wound healing.[41,44] Recently emerging evidence supports the hypothesis that dysfunction of microglia, the counterpart of macrophages in the brain, plays important roles in the pathogenesis of AD.[45–47] Therefore, downregulation of genes specific to oligodendrocytes and microglial cells in the *ob/ob* background might increase susceptibility to Aβ accumulation.

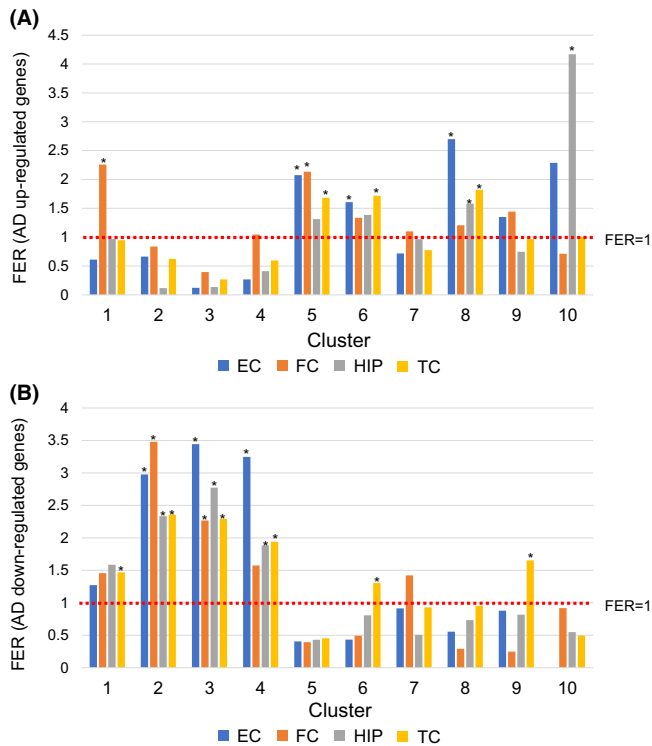On the other hand, genes specific to astrocytes and microglial cells were upregulated in *APP* mice (Figure 3),

(A)

(B)

FIGURE 4 Enrichment analysis of differentially expressed genes (DEGs) in Alzheimer's disease (AD). Evaluation of number of genes with upregulated expression (A) and downregulated expression (B) in brains from patients with AD depending on brain regions. The y-axis shows the fold enrichment ratio (FER), which indicates the ratio of the number of DEGs to the expected number. A FER of greater than one indicates that the proportion of DEGs is higher than the expected proportion. The asterisks indicate the FERs satisfying the criteria of FER >1 and FDR-adjusted $p < 0.05$. p-values were calculated by the hypergeometric test. The red line indicates an FER of 1. EC: entorhinal cortex, FC: frontal cortex, HIP: hippocampus, TC: temporal cortex

consistent with previous reports. By contrast, those genes were not upregulated in *APP*;*ob*/*ob* mice, probably because Aβ levels are lower in *APP*;*ob*/*ob* mice than in *APP* mice at 16 months of age. Several neuropathological studies have revealed that patients with AD who have been diagnosed with diabetes exhibit decreased amyloid accumulation compared with patients without diabetes,[14–16] while several neuropathological studies reported no association between diabetes and amyloid accumulation.[10–13] In our analysis of the National Alzheimer's Coordinating Center (NACC, in the United States) database, diabetes was associated with decreased amyloid accumulation, and the difference was especially significant in *APOE3* carriers.[17] Consistent with this finding, we recently reported that Aβ levels were decreased in male *APP* knock-in *ob*/*ob* mice compared with *APP* knock-in mice.[48] In the current study, we also observed that the expression level of *APP* was reduced in *APP*;*ob*/*ob* mice compared with *APP* mice, although the mechanism

underlying this difference is unclear. Future studies are required to investigate whether *APP* expression is reduced by obesity/diabetes in humans.

Most importantly, we identified a cluster, cluster 10, that contained genes upregulated in *APP*;*ob*/*ob* mice but not in either *APP* or *ob*/*ob* mice. Genes upregulated in the brains of humans with AD, especially the hippocampal area, were enriched in cluster 10. Interestingly, genes in cluster 10 formed a network, and the upregulated genes partially overlapped with those in a cell model of neurodegeneration[28] and the animal models of neurological disorders, such as ischemia models[29] and an epilepsy model.[30] Zhang et al. identified a genomic program in hippocampal neurons that mediates synaptic activity-induced, acquired neuroprotection; this program includes B-cell translocation gene 2 (Btg2), Cyr61, Dusp1, and JunB.[28] Btg2 is involved in regulating the proliferation of inflammatory cells, and Cyr61 is essential for angiogenesis.[49,50] These molecules might be related to the inflammatory and vascular phenotypes, respectively, in these mice, as we previously reported.[21] In addition, we found that the transcription factor SRF might be a common transcriptional regulator for some genes in cluster 10. Interestingly, a recent single-cell analysis of human postmortem brain tissue suggested that SRF can control the conversion from healthy cells to AD cells.[51] Moreover, the transcriptional activity of SRF is reported to be increased in the skeletal muscle of patients with type 2 diabetes with a family history, and pharmacological inhibition of SRF improves insulin resistance in animal models.[52] Additionally, conditional genetic ablation of SRF diminishes epilepsy-associated neurodegeneration in the abovementioned epilepsy model.[30] Seizures, a major symptom of epilepsy, are an early symptom of autosomaldominant AD.[27] Therefore, further examination is needed to validate the importance of genes involved in cluster 10 in the interaction between obesity/diabetes and AD.

Our animal models have several limitations. In this study, we selected *APP* transgenic mice as a model of AD and *ob*/*ob* mice as a model of diabetes-linked obesity. *APP* transgenic mice overexpress *APP*, and *ob*/*ob* mice become obese and mildly diabetic resulting from leptin deficiency. In future studies, we will study the interaction between obesity/diabetes and AD in both humans and other animal models. Also, we did not fully characterize phenotypes of *APP*;*ob*/*ob* mice at 16 months of age, while they showed cognitive changes at young age and vascular changes at 12 months of age.[21] Together with the reduction of their Aβ levels at 16 months of age, genes upregulated in *APP*;*ob*/*ob* mice indeed might contribute to some biological defense against AD insults, rather than synergistic harmful effects. Further studies would be necessary to address the roles of these upregulated genes.

The upregulated expression of a subset of genes in *APP*;*ob*/*ob* mice provides a clue to understand the

FIGURE 5 Analysis of cluster 10. (A) Validation of gene expression patterns in cluster 10 by real-time PCR; the mRNA levels of *Btg2*, *Cyr61*, *JunB*, *Lss*, *Dusp1*, *Fos* and *Npas4* were measured using real-time PCR and were compared among the genotypes (*n* = 4–6 mice/group). The data are presented as the adjusted means ± standard errors of the mean. *$p < 0.05$, **$p < 0.01$, and ***$p < 0.001$ by the Tukey–Kramer test. Wt = wild-type. (B) The network shows the relationships between TFs and their target genes. The orange nodes represent TFs with a z-score of ≥10 and a Fisher score of ≥7 (default values) in "Mouse Single Site Analysis" in oPOSSUM. The blue nodes represent cluster 10 genes that contain binding motifs for the linked TFs. The node size of the TF indicates the magnitude of the FER

interaction between diabetes-linked obesity and AD. An understanding of the precise mechanisms underlying this interaction will likely provide novel therapeutic targets for obesity/diabetes and AD. Further studies are required to determine the precise contributions of these genes to the pathogenesis of AD and obesity/diabetes *in vitro* and *in vivo*.

CONFLICT OF INTERESTS

The authors have no conflicts of interest related to the content of this article to declare.

AUTHORS' CONTRIBUTIONS

Conceptualization: N. S.; Methodology: M. S., M. K., and N. S.; Bioinformatic Analysis: M. K.; Histological analysis: Y. T. and K. S.; Other investigation: M. S., M. O. T., Y. N., S. T., M. M., S. N., A. F., and N. S.; Writing-Original Draft: M. S., M. K., and N. S.; Funding Acquisition: M. S., and N. S.; Supervision: R. M., A. N., and N. S. All authors have read and approved the final manuscript.

REFERENCES

1. Roberts RO, Knopman DS, Przybelski SA, et al. Association of type 2 diabetes with brain atrophy and cognitive impairment. *Neurology*. 2014;82:1132-1141.
2. Morris JK, Vidoni ED, Honea RA, Burns JM. Impaired glycemia increases disease progression in mild cognitive impairment. *Neurobiol Aging*. 2014;35:585-589.
3. Maher PA, Schubert DR. Metabolic links between diabetes and Alzheimer's disease. *Expert Rev Neurother*. 2009;9:617-630.
4. Kopf D, Frolich L. Risk of incident Alzheimer's disease in diabetic patients: a systematic review of prospective trials. *J Alzheimers Dis*. 2009;16:677-685.
5. Ott A, Stolk RP, van Harskamp F, Pols HA, Hofman A, Breteler MM. Diabetes mellitus and the risk of dementia: the Rotterdam Study. *Neurology*. 1999;53:1937-1942.
6. Matsuzaki T, Sasaki K, Tanizaki Y, et al. Insulin resistance is associated with the pathology of Alzheimer disease: the Hisayama study. *Neurology*. 2010;75:764-770.
7. Leibson CL, Rocca WA, Hanson VA, et al. Risk of dementia among persons with diabetes mellitus: a population-based cohort study. *Am J Epidemiol*. 1997;145:301-308.
8. Shinohara M, Sato N. Bidirectional interactions between diabetes and Alzheimer's disease. *Neurochem Int*. 2017;108:296-302.
9. Sutherland GT, Lim J, Srikanth V, Bruce DG. Epidemiological approaches to understanding the link between type 2 diabetes and dementia. *J Alzheimers Dis*. 2017;59:393-403.
10. Heitner J, Dickson D. Diabetics do not have increased Alzheimer-type pathology compared with age-matched control subjects. A retrospective postmortem immunocytochemical and histofluorescent study. *Neurology*. 1997;49:1306-1311.
11. Arvanitakis Z, Schneider JA, Wilson RS, et al. Diabetes is related to cerebral infarction but not to AD pathology in older persons. *Neurology*. 2006;67:1960-1965.
12. Abner EL, Nelson PT, Kryscio RJ, et al. Diabetes is associated with cerebrovascular but not Alzheimer's disease neuropathology. *Alzheimers Dement*. 2016;12:882-889.
13. Dos Santos Matioli MNP, Suemoto CK, Rodriguez RD, et al. Diabetes is not associated with Alzheimer's disease neuropathology. *J Alzheimers Dis*. 2017;60:1035-1043.
14. Kalaria RN. Neurodegenerative disease: diabetes, microvascular pathology and Alzheimer disease. *Nat Rev Neurol*. 2009;5:305-306.
15. Beeri MS, Silverman JM, Davis KL, et al. Type 2 diabetes is negatively associated with Alzheimer's disease neuropathology. *J Gerontol A Biol Sci Med Sci*. 2005;60:471-475.
16. Nelson PT, Smith CD, Abner EA, et al. Human cerebral neuropathology of Type 2 diabetes mellitus. *Biochim Biophys Acta*. 2009;1792:454-469.
17. Shinohara M, Tashiro Y, Suzuki K, Fukumori A, Bu G, Sato N. Interaction between APOE genotype and diabetes in cognitive decline. *Alzheimer's Dement Diagn Assessm Dis Monit*. 2020;12:e12006.
18. Sato N, Morishita R. Brain alterations and clinical symptoms of dementia in diabetes: abeta/tau-dependent and independent mechanisms. *Front Endocrinol (Lausanne)*. 2014;5:143.
19. Anstey KJ, Cherbuin N, Budge M, Young J. Body mass index in midlife and late-life as a risk factor for dementia: a meta-analysis of prospective studies. *Obes Rev*. 2011;12:e426-e437.
20. Ngandu T, Lehtisalo J, Solomon A, et al. A 2 year multidomain intervention of diet, exercise, cognitive training, and vascular risk monitoring versus control to prevent cognitive decline in at-risk elderly people (FINGER): a randomised controlled trial. *Lancet*. 2015;385(9984):2255-2263.
21. Takeda S, Sato N, Uchio-Yamada K, et al. Diabetes-accelerated memory dysfunction via cerebrovascular inflammation and Abeta deposition in an Alzheimer mouse model with diabetes. *Proc Natl Acad Sci USA*. 2010;107:7036-7041.
22. Sato N, Takeda S, Uchio-Yamada K, et al. Role of insulin signaling in the interaction between Alzheimer disease and diabetes mellitus: a missing link to therapeutic potential. *Curr Aging Sci*. 2011;4:118-127.
23. Sturchler-Pierrat C, Abramowski D, Duke M, et al. Two amyloid precursor protein transgenic mouse models with Alzheimer disease-like pathology. *Proc Natl Acad Sci*. 1997;94:13287-13292.
24. Pelleymounter M, Cullen M, Baker M, et al. Effects of the obese gene product on body weight regulation in ob/ob mice. *Science*. 1995;269:540-543.

25. Halaas J, Gajiwala K, Maffei M, et al. Weight-reducing effects of the plasma protein encoded by the obese gene. *Science*. 1995;269:543-546.

26. Campfield L, Smith F, Guisez Y, Devos R, Burn P. Recombinant mouse OB protein: evidence for a peripheral signal linking adiposity and central neural networks. *Science*. 1995;269:546-549.

27. Voglein J, Noachtar S, McDade E, et al. Seizures as an early symptom of autosomal dominant Alzheimer's disease. *Neurobiol Aging*. 2019;76:18-23.

28. Zhang SJ, Zou M, Lu L, et al. Nuclear calcium signaling controls expression of a large gene pool: identification of a gene program for acquired neuroprotection induced by synaptic activity. *PLoS Genet*. 2009;5:e1000604.

29. Ohtomo R, Bannai T, Ohtomo G, et al. Cilostazol alleviates white matter degeneration caused by chronic cerebral hypoperfusion in mice: implication of its mechanism from gene expression analysis. *Neurosci Lett*. 2018;662:247-252.

30. Losing P, Niturad CE, Harrer M, et al. SRF modulates seizure occurrence, activity induced gene transcription and hippocampal circuit reorganization in the mouse pilocarpine epilepsy model. *Mol Brain*. 2017;10:30.

31. Tibshirani R, Walther G, Hastie T. Estimating the number of clusters in a data set via the gap statistic. *J R Stat Soc Ser B (Stat Methodol)*. 2001;63:411-423.

32. Team RC. Computing RFfS: R: a language and environment for statistical computing. In: *Book R: A Language and Environment for Statistical Computing* (Editor ed.^eds.). City; 2019.

33. Zhang Y, Chen K, Sloan SA, et al. An RNA-sequencing transcriptome and splicing database of glia, neurons, and vascular cells of the cerebral cortex. *J Neurosci*. 2014;34:11929-11947.

34. Ho Sui SJ, Mortimer JR, Arenillas DJ, et al. oPOSSUM: identification of over-represented transcription factor binding sites in co-expressed genes. *Nucleic Acids Res*. 2005;33:3154-3164.

35. Shinohara M, Fujioka S, Murray ME, et al. Regional distribution of synaptic markers and APP correlate with distinct clinicopathological features in sporadic and familial Alzheimer's disease. *Brain*. 2014;137:1533-1549.

36. Moran C, Phan TG, Chen J, et al. Brain atrophy in type 2 diabetes: regional distribution and influence on cognition. *Diabetes Care*. 2013;36:4036-4042.

37. Garcia-Casares N, Berthier ML, Jorge RE, et al. Structural and functional brain changes in middle-aged type 2 diabetic patients: a cross-sectional study. *J Alzheimers Dis*. 2014;40:375-386.

38. Chen YC, Jiao Y, Cui Y, et al. Aberrant brain functional connectivity related to insulin resistance in type 2 diabetes: a resting-state FMRI study. *Diabetes Care*. 2014;37:1689-1696.

39. Hoogenboom WS, Marder TJ, Flores VL, et al. Cerebral white matter integrity and resting-state functional connectivity in middle-aged patients with type 2 diabetes. *Diabetes*. 2014;63:728-738.

40. Lossos A, Elazar N, Lerer I, et al. Myelin-associated glycoprotein gene mutation causes Pelizaeus-Merzbacher disease-like disorder. *Brain*. 2015;138:2521-2536.

41. Falanga V. Wound healing and its impairment in the diabetic foot. *Lancet*. 2005;366:1736-1743.

42. Shultz LD, Schweitzer PA, Christianson SW, et al. Multiple defects in innate and adaptive immunologic function in NOD/LtSz-scid mice. *J Immunol*. 1995;154:180-191.

43. Ratter JM, Tack CJ, Netea MG, Stienstra R. Environmental signals influencing myeloid cell metabolism and function in diabetes. *Trends Endocrinol Metab*. 2018.

44. Dinh T, Tecilazich F, Kafanas A, et al. Mechanisms involved in the development and healing of diabetic foot ulceration. *Diabetes*. 2012;61:2937-2947.

45. Guerreiro R, Wojtas A, Bras J, et al. TREM2 variants in Alzheimer's disease. *N Engl J Med*. 2012;368:117-127.

46. Jonsson T, Stefansson H, Steinberg S, et al. Variant of TREM2 associated with the risk of Alzheimer's disease. *N Engl J Med*. 2012;368:107-116.

47. Hansen DV, Hanson JE, Sheng M. Microglia in Alzheimer's disease. *J Cell Biol*. 2018;217:459.

48. Shinohara M, Tashiro Y, Shinohara M, et al. Increased levels of Aβ42 decrease the lifespan of ob/ob mice with dysregulation of microglia and astrocytes. *FASEB J*. 2020;34:2425-2435.

49. Babic AM, Kireeva ML, Kolesnikova TV, Lau LF. CYR61, a product of a growth factor-inducible immediate early gene, promotes angiogenesis and tumor growth. *Proc Natl Acad Sci*. 1998;95:6355-6360.

50. Yuniati L, Scheijen B, van der Meer LT, van Leeuwen FN. Tumor suppressors BTG1 and BTG2: beyond growth control. *J Cell Physiol*. 2019;234:5379-5389.

51. Grubman A, Chew G, Ouyang JF, et al. A single-cell atlas of entorhinal cortex from individuals with Alzheimer's disease reveals cell-type-specific gene expression regulation. *Nat Neurosci*. 2019;22:2087-2097.

52. Jin W, Goldfine AB, Boes T, et al. Increased SRF transcriptional activity in human and mouse skeletal muscle is a signature of insulin resistance. *J Clin Investig*. 2011;121:918-929.

SUPPORTING INFORMATION

Additional supporting information may be found online in the Supporting Information section.